J Mater Sci: Mater Electron (2015) 26:134–138
DOI 10.1007/s10854-014-2374-4

Effects of barium substitution on the dielectric properties of $Sr(Fe_{0.5}Nb_{0.5})O_3$ ceramics

Zhuo Wang · Hai Juan Li · Liang Liang Zhang · Yong Fei Wen · Yong Ping Pu

Received: 24 July 2014 / Accepted: 6 October 2014 / Published online: 11 October 2014

Abstract The Ba-substituted $Sr_{1-x}Ba_x(Fe_{0.5}Nb_{0.5})O_3$ (SBFN, $x = 0$, 0.2, 0.5, 0.8) ceramics were prepared by a conventional solid-state sintering, and their microstructure and dielectric properties were investigated. The single-phase SBFN were obtained up to $x = 0.8$ Ba substitution and the lattice parameter increased with Ba substitution concentration. The dielectric constant increased with Ba substitution, and the highest value of $\sim$180,000 was observed in the $x = 0.8$ Ba-substituted specimen at 1 kHz. Besides, the dielectric constant increased rapidly a giant value more than 10^6 over a broad temperature range for $x = 0.8$ Ba-substituted specimen. The obtained electric and dielectric properties in Ba-substituted SBFN were discussed in terms of the internal barrier layer capacitor model and electrode response.

1 Introduction

A number of Fe-containing complex perovskites $A(Fe_{0.5}B_{0.5})O_3$ (A = Ca, Ba, Sr; B = Nb, Ta, Sb) [1–5] have attracted considerable attention because of their giant dielectric response and the unique dielectric relaxation behavior similar to that in $CaCu_3Ti_4O_{12}$ [6, 7]. The common feature of these materials is a high dielectric permittivity (in the order of 10^3–10^5) over a broad temperature and frequency interval, and a sharp decrease of permittivity with increasing the frequency or decreasing the temperature to a critical point without any detectable phase transition. These materials play important role in microelectronics and have various technological applications, such as multilayer capacitors, microwave frequency resonators, sensors, detectors, memory devices and actuators. Among these materials, $Sr(Fe_{0.5}Nb_{0.5})O_3$ (SFN) is a relaxor-type ferroelectric material which has a partially disordered perovskite structure [3, 8]. The Fe^{3+} and Nb^{5+} ions are randomly distributed in the octahedral positions and have small lattice distortion. The high dielectric constant of SFN ceramics were interpreted by the Maxwell–Wagner mechanism in the previous work [3, 8]. But the extrinsic mechanism of the dielectric response in SFN ceramics is not very clear so far, and dielectric constant of SFN ceramics is not great enough such as $CaCu_3Ti_4O_{12}$.

Recently, more work based on ion substitution at A-site in complex perovskite materials has been carried out in order to improve the dielectric properties and deepen understanding of the extrinsic mechanism of giant dielectric response for these materials [9–12]. On the one hand, $Ba(Fe_{0.5}Nb_{0.5})O_3$ (BFN) -based dielectrics are more focused in research field, due to have an extraordinarily high dielectric constant of $\varepsilon_r \approx 10^4$–$10^5$ at a low frequency region [3, 4]. On the other hand, both BFN and SFN are described as typical perovskite-type compounds and could be expected to form the solid solutions. BFN and SFN may fully achieve solid solution due to the difference of ionic radius of Ba^{2+} ions ($r(Ba^{2+})$ = 1.35 Å) and Sr^{2+} ions ($r(Sr^{2+})$ = 1.18 Å) is less than 15 %. In view of the above, BFN was incorporated into SFN may increase the dielectric constant and the extrinsic mechanism of the high dielectric response becomes much clearer than before.

In this paper, the effects of barium substituting on the SFN samples prepared according to the formula $Sr_{1-x}Ba_x(Fe_{0.5}Nb_{0.5})O_3$ ($x = 0$, 0.2, 0.5, 0.8) were systematic investigated. The phase structure, dielectric properties and corresponding impedance of SBFN ceramics were investigated.

Z. Wang (✉) · H. J. Li · L. L. Zhang · Y. F. Wen · Y. P. Pu
School of Materials Science and Engineering, Shaanxi University of Science and Technology, Xi'an 710021, China
e-mail: wangzhuo@sust.edu.cn

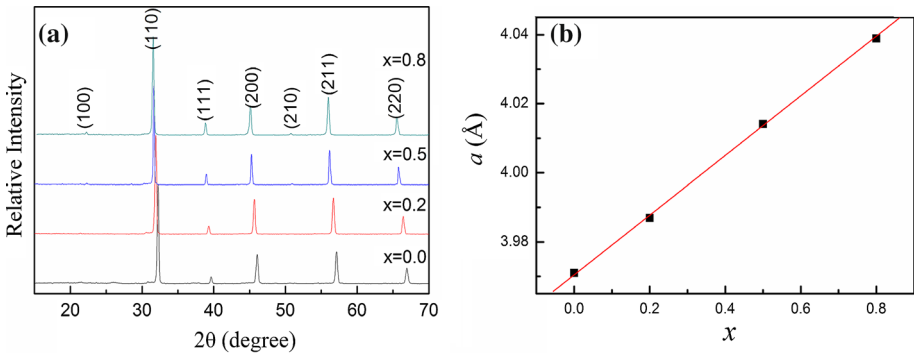

Fig. 1 **a** XRD patterns of $Sr_{1-x}Ba_x(Fe_{0.5}Nb_{0.5})O_3$ ($x = 0$, 0.2, 0.5, 0.8) ceramics sintered at 1,400 °C for 3 h. **b** Lattice parameters of $Sr_{1-x}Ba_x(Fe_{0.5}Nb_{0.5})O_3$ as a function of barium substitution. The *solid lines* are results of the linear fitting

2 Experimental

$Sr_{1-x}Ba_x(Fe_{0.5}Nb_{0.5})O_3$ ($x = 0$, 0.2, 0.5, 0.8) ceramics were synthesized by the conventional solid-state reaction method, using high purity $SrCO_3$ (99 %), $BaCO_3$ (99 %), Fe_2O_3 (99 %), and Nb_2O_5 (99.99 %) powders as raw materials, which were carefully weighted and mixed throughly. Stoichiometric amounts of the raw powders were ball-milled in a polyethylene jar with ZrO_2 media in distilled water for 4 h and calcined at 1,100 °C in air for 3 h. The calcined powders were then reground and pressed into cylindrical compacts of 11–12 mm in diameter and 2 mm in thickness under a pressure of about 98 MPa. These pressed samples were sintered at 1,400 °C in air for 3 h to obtain desired and dense ceramics for $Sr_{1-x}Ba_x(Fe_{0.5}Nb_{0.5})O_3$. The electrodes for measurements were deposited on the ground disk surface by rubbing on silver.

The density of the sintered samples was measured using Archimedes' method. The relative densities are above 95 % of theoretical densities for SBFN ceramics. The phase purity, structure and lattice parameters of the sample were determined by X-ray powder diffraction with Cu $K\alpha$ radiation at room temperature (D/max-2200PC). The dielectric characteristics of these samples were conducted on the silver pasted samples in broad temperature and frequency (20 Hz–2 MHz) ranges with a broadband dielectric spectrometer (Agilent-E4980A).

3 Results and discussion

Figure 1a shows the XRD patterns of $Sr_{1-x}Ba_x(Fe_{0.5}Nb_{0.5})O_3$ ($x = 0$, 0.2, 0.5, 0.8) ceramics sintered at 1,400 °C for 3 h. All the diffraction peaks in the X-ray diffraction patterns are confirmed to indicate the cubic crystal structure in the space group $pm\bar{3}m(221)$, and no secondary phase was observed. Besides, it can be seen that the diffraction peaks shift towards lower angle with Ba substitution concentration. The lattice parameters of all SBFN samples are represented in Fig. 1b. As shown in Fig. 1b, the lattice constant increased linearly with Ba substitution, it revealed that the Ba substitution for Sr actually occurred during sintering. The increased lattice constant can be attributed to the ionic radius difference between Sr and Ba ions ($r(Ba^{2+})$ = 1.35 Å and $r(Sr^{2+})$ = 1.18 Å). The above phenomena also indicated that barium ions have completely entered into the strontium sites improved the dielectric properties of SFN ceramics.

Figure 2 shows the SEM surface micrographs of the $Sr_{1-x}Ba_x(Fe_{0.5}Nb_{0.5})O_3$ ($x = 0$, 0.2, 0.5, 0.8) ceramics, which were at their maximum densities. As seen from Fig. 2, when adding the Ba substitution, the grain sizes of samples increased significantly. The Ba substitution for Sr effectively promoted the grain growth. This increase in the grain size is expected to influence the dielectric properties of SBFN ceramics as the grain size is an important parameter in internal barrier layer capacitor model [13].

Figure 3 shows the frequency dependence of the dielectric constant and dielectric loss of $Sr_{1-x}Ba_x(Fe_{0.5}Nb_{0.5})O_3$ ($x = 0$, 0.2, 0.5, 0.8) ceramics at room temperature. As shown in Fig. 3a, for all the samples the dielectric constant decreases with increasing frequency, which is a normal behavior of dielectrics. Higher values of ε' at lower frequencies are due to the presence of different types of polarization (dipolar, atomic, ionic, electronics and Maxwell–Wagner polarizations) in the materials. At higher frequencies, some of the above-mentioned polarizations cannot follow the alternating field and may have less contribution to dielectric constant [14]. In addition, we can seen that the ε' of SBFN ceramics increases with increasing x. It is to be noted that a giant ε' ($\sim$180,000) was observed for the $x = 0.8$ sample at 1 kHz. Based on the IBLC model, the effective dielectric constant (ε_{eff}) is inversely proportional to the ratio of thickness of the insulating layer (grain boundary) (t_{gb}) to the grain size (t_g) as expressed $\varepsilon_{eff} \sim 1/(t_{gb}/t_g)$. Therefore, the increase of ε' in SBFN ceramics was attributed to the decrease of the ratio of grain boundary thickness to grain size. It is clear that ε' is strongly dependent on the microstructure and can be maximized by enhancing the the grain size (t_g), or by

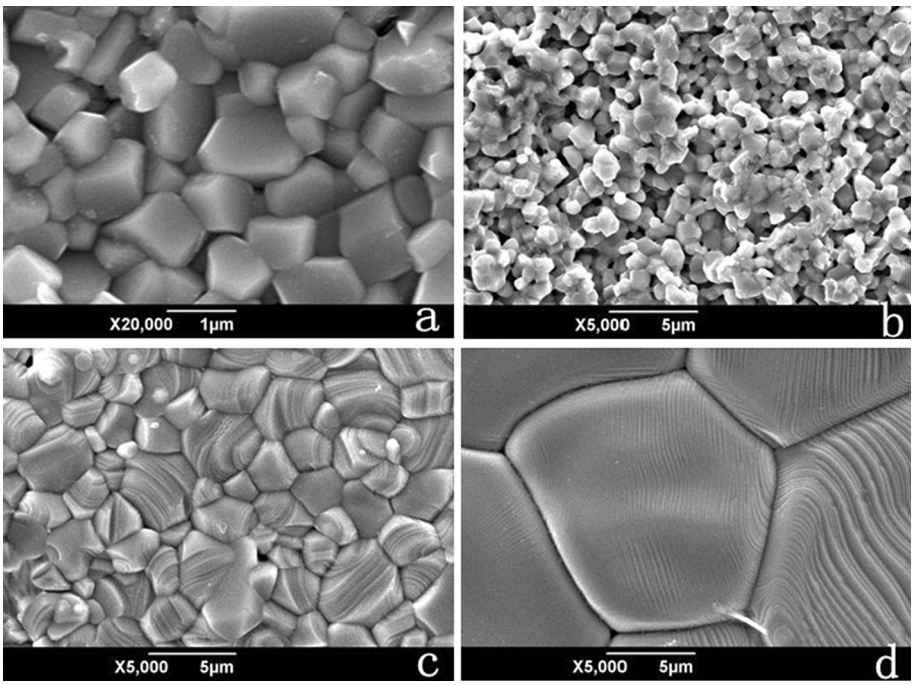

Fig. 2 SEM surface micrographs of the $Sr_{1-x}Ba_x(Fe_{0.5}Nb_{0.5})O_3$ ceramics (**a** $x = 0$, **b** $x = 0.2$, **c** $x = 0.5$ and **d** $x = 0.8$)

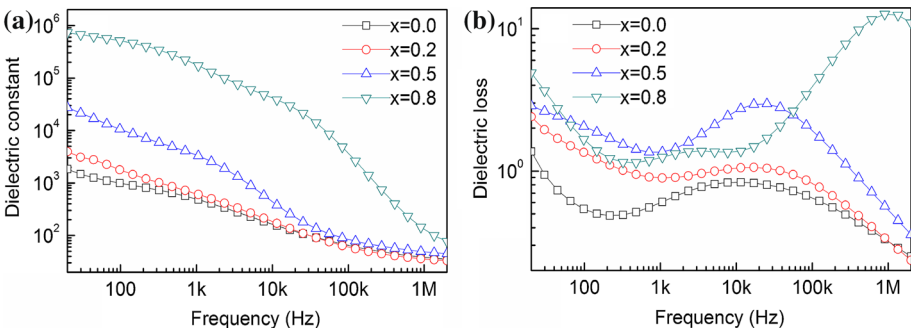

Fig. 3 Frequency dependence of the dielectric constants and dielectric loss for $Sr_{1-x}Ba_x(Fe_{0.5}Nb_{0.5})O_3$ ($x = 0$, 0.2, 0.5, 0.8) ceramics at room temperature

thinning down the grain boundary (t_{gb}) with high dielectric constant. In general, the grain boundary (t_{gb}) has very small change [15, 16]. So the increase of ε' in SBFN ceramics was attributed to the increase of the grain size, which is consistent with the result of SEM. In Fig. 3b, the tanδ shows a relaxation peak while increasing the frequency to a certain value the ε' shows a step decrease.

Figure 4 shows the temperature dependence of the dielectric constants for $Sr_{1-x}Ba_x(Fe_{0.5}Nb_{0.5})O_3$ ($x = 0$, 0.2, 0.5, 0.8) ceramics at 1 kHz. The ε' of SBFN ceramics increased with Ba substitution. For $x = 0$ the dielectric constant increase with rise in temperature. The reason might be the increased conductivity in the samples caused by the presence of Fe^{2+} in sintered ceramics, as suggested by Ananta and Thomas [17]. The concentration of Fe^{2+} ions is known to be very sensitive to temperature, and it increases as temperature increases [18]. It is known that the co-existence of Fe^{2+} and Fe^{3+} ions on equivalent crystallographic sites can give rise to an electron hopping conduction mechanism. Due to the finite hopping probability of electrons, this conduction mechanism tends to come into effect only at lower frequencies. This characteristic has been observed in other complex perovskites such as $Ba(Fe_{0.5}Nb_{0.5})O_3$ and $Ba(Fe_{0.5}Ta_{0.5})O_3$ [19, 20]. Moreover, the ε' increases rapidly a giant value more than 10^6 over a broad temperature range for $x = 0.8$. It should be noted that the ε' is quite great compared with many giant dielectric materials such as $CaCu_3Ti_4O_{12}$, $Ba(Fe_{0.5}Nb_{0.5})O_3$ and $Ba(Fe_{0.5}Ta_{0.5})O_3$ [1, 21, 22].

In order to understand further extrinsic effects of the dielectric behavior of SBFN ceramics, we have analyzed the complex impedance spectra of $Sr_{0.2}Ba_{0.8}(Fe_{0.5}Nb_{0.5})O_3$ ceramics at various temperatures. Figure 5 shows the variation of imaginary part of impedance (Z'') as a function of real part (Z') at 303, 373, 423 and 473 K. It is very clear that two overlapped semicircular arcs can be discerned in

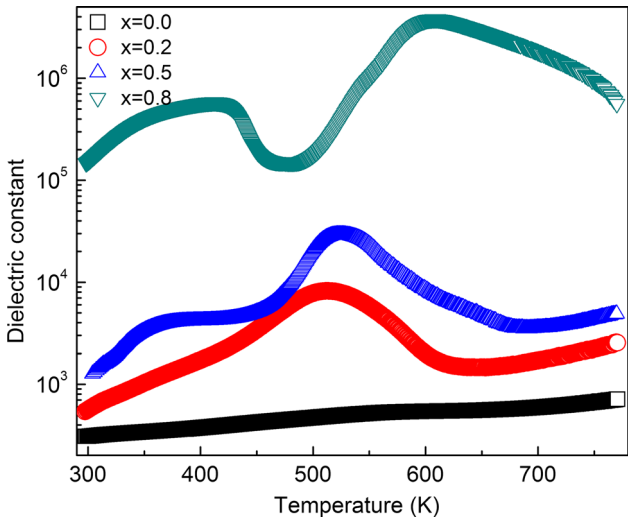

Fig. 4 Temperature dependence of the dielectric constants for $Sr_{1-x}Ba_x(Fe_{0.5}Nb_{0.5})O_3$ ($x = 0$, 0.2, 0.5, 0.8) ceramics measured at 1 kHz

the plots. The small one in high frequency region has non-zero intercept at the high frequency side. The equivalent circuit for the impedance data therefore may be two sets of parallel RC elements (corresponding to the two semicircular arc) in series, which then connect with a single R element (corresponding to the high frequency intercept of the small semicircular arc) in series. The calculated capacitances values are 10^{-8} (the small semicircular arc) and 10^{-7} (the large semicircular arc) F cm^{-1}, respectively. The capacitances values vary slightly in the considered temperature range. Based on the brickwork layer model for electroceramics, the high frequency intercept of the small semicircular arc and the small semicircular arc are attributed to bulk and grain boundary responses, respectively [23–25]. The larger semicircular arc at low frequency could be mainly attributed to the electrode response. The reason is that the sliver electrode could induce significant contact resistivity, showing semicircular arcs and larger capacitances [26]. The electrode response depends on the electrode and the conductivity of the ceramics [27]. Meanwhile, the plot reveals grain interiors resistance (R_g) of about 120, 25, 11 and 6.5 Ω, and grain boundaries resistance (R_{gb}) of about 900, 103, 35 and 11 Ω, respectively. These features imply an equivalent circuit consisting of a larger resistive grain boundary and a smaller resistive grain. As shown in Fig. 5b, both R_g and R_{gb} obtained from fitting the Cole–Cole plots obey the Arrhenius law.

$$R = R_0 \exp\left(E_a/k_B T\right) \quad (1)$$

where R_0 is the pre-exponential term and E_a is the activation energy. The linear relationship between the resistances and temperature is observed when the temperature is in the range of 303–473 K. Using the Eq. (1), the activation energies for grain interiors and grain boundaries are 0.21 and 0.32 eV, respectively. This study demonstrates that the giant dielectric constant observed in $Sr_{0.2}Ba_{0.8}(Fe_{0.5}Nb_{0.5})O_3$ ceramics as barrier layer capacitance elements within the ceramics and electrode response.

4 Conclusions

$Sr_{1-x}Ba_x(Fe_{0.5}Nb_{0.5})O_3$ ($x = 0$, 0.2, 0.5, 0.8) ceramics were synthesized by the conventional solid-state reaction method. X-ray diffraction analysis revealed that the single-phase SBFN were obtained up to $x = 0.8$ Ba substitution and the lattice parameter increased with Ba substitution concentration. The dielectric constant increased with Ba substitution, and the highest value of ~180,000 was observed in the $x = 0.8$ Ba-substituted specimen at 1 kHz. Based on the IBLC model, the increase of ε' in SBFN ceramics was attributed to the decrease of the ratio of grain boundary thickness to grain size. Besides, the dielectric constant increased rapidly a giant value more than 10^6 over a broad temperature range for $x = 0.8$, and the Impedance complex plane plots concluded that the giant dielectric constant observed in $Sr_{0.2}Ba_{0.8}(Fe_{0.5}Nb_{0.5})O_3$ ceramics as

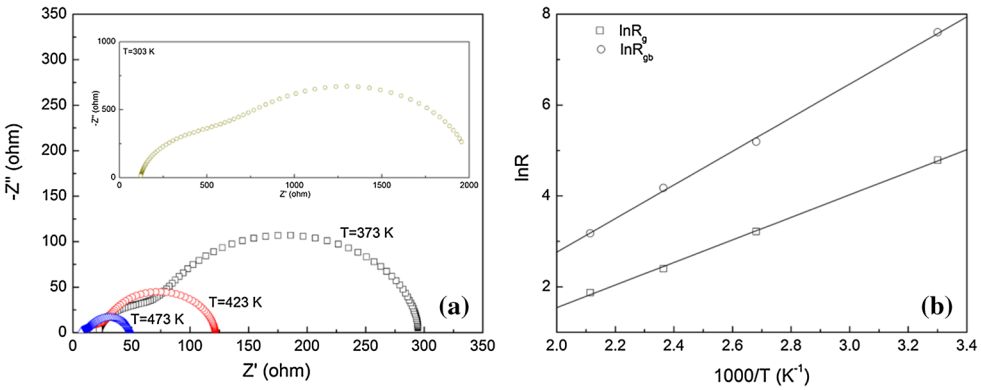

Fig. 5 **a** Complex impedance spectra of $Sr_{0.2}Ba_{0.8}(Fe_{0.5}Nb_{0.5})O_3$ ceramics at various temperatures. **b** Resistances of grain interiors and grain boundaries for $Sr_{0.2}Ba_{0.8}(Fe_{0.5}Nb_{0.5})O_3$ ceramics. The *solid lines* are results of thermally activated hopping fitting

barrier layer capacitance elements and electrode response. These results suggest that barium ions occupied the strontium sites improved the dielectric properties of $Sr(Fe_{0.5}Nb_{0.5})O_3$ ceramics.

Acknowledgments The present work was supported by National Science Foundation of China (51372144, 51102159), the Scientific Research Foundation for Ph.D (BJ10-16), the Academic Backbones Cultivation Program (XS11-02) and Graduate Innovation Fund of Shaanxi University of Science and Technology.

References

1. S. Saha, T.P. Sinha, J. Phys.: Condens. Matter **14**, 249–258 (2002)
2. Z. Wang, H.J. Li, L.L. Zhang, Y.P. Pu, J. Mater. Sci.: Mater. Electron. **24**, 3418–3422 (2013)
3. I.P. Raevski, S.A. Prosandeev, A.S. Bogatin, M.A. Malitskaya, L. Jastrabik, J. Appl. Phys. **93**, 4130–4136 (2003)
4. C.Y. Chung, Y.H. Chang, G.J. Chen, J. Appl. Phys. **96**, 6624–6628 (2004)
5. C.C. Homes, T. Vogt, S.M. Shapiro, S. Wakimoto, A.P. Ramirez, Science **293**, 673–676 (2001)
6. B. Wang, Y.P. Pu, H.D. Wu, K. Chen, N. Xu, Ceram. Inter. **39**, S525–S528 (2013)
7. B. Wang, Y.P. Pu, H.D. Wu et al., J. Mater. Sci.: Mater. Electron. **23**, 612–617 (2012)
8. S. Saha, T.P. Sinha, J. Appl. Phys. **99**, 014109 (2006)
9. H. Abdelkefi, H. Khemakhem, G. Vélu, J.C. Carru, R.V. Mühll, J. Alloys Compd. **399**, 1–6 (2005)
10. C.L. Fu, C.R. Yang, H.W. Chen, Y.X. Wang, L.Y. Hu, Mater. Sci. Eng., B **119**, 185–188 (2005)
11. C.Y. Chung, Y.S. Chang, G.J. Chen, C.C. Chung, T.W. Huang, Solid State Commun. **145**, 212–217 (2008)
12. K.F. Liao, Y.S. Chang, Y.L. Chai, Y.Y. Tsai, H.L. Chen, Mater. Sci. Eng., B **172**, 300–304 (2010)
13. B.S. Prakash, K.B.R. Varma, J. Solid State Chem. **180**, 1918–1927 (2007)
14. Y. Lin, Z.F. Zhu, H.B. Yang, Mater. Manuf. Processes **26**, 632–635 (2011)
15. T.B. Adams, D.C. Sinclair, A.R. West, J. Am. Ceram. Soc. **89**, 3129–3135 (2006)
16. T.B. Adams, D.C. Sinclair, A.R. West, Adv. Mater. **14**, 1321–1323 (2002)
17. S. Ananta, N.W. Thomas, J. Eur. Ceram. Soc. **19**, 1873–1881 (1999)
18. K. Singh, S.A. Band, W.K. Kinge, Ferroelectrics **306**, 179–185 (2004)
19. Z. Wang, X.M. Chen, L. Ni, X.Q. Liu, Appl. Phys. Lett. **90**, 022904 (2007)
20. Z. Wang, X.M. Chen, L. Ni, Y.Y. Liu, X.Q. Liu, Appl. Phys. Lett. **90**, 102905 (2007)
21. S. Kwon, C.C. Huang, E.A. Patterson, D.P. Cann, E.F. Alberta, S. Kwon, W.S. Hackenberger, D.P. Cann, Mater. Lett. **62**, 633–636 (2008)
22. A. Dutta, T.P. Sinha, Mater. Res. Bull. **46**, 518–524 (2011)
23. J.T.S. Irvine, D.C. Sinclair, A.R. West, Adv. Mater. **2**, 132–138 (1990)
24. X.J. Kuang, C. Bridges, M. Allix et al., Chem. Mater. **18**, 5130–5136 (2006)
25. P. Lunkenheimer, R. Fichtl, S.G. Ebbinghaus, A. Loidl, Phys. Rev. B **70**, 172102 (2004)
26. X.J. Kuang, H. Zhu, M. Allix et al., J. Mater. Chem. **22**, 8103–8109 (2012)
27. L. Miranda, D.C. Sinclair, M. Hernando et al., Chem. Mater. **22**, 4320–4327 (2010)